Study on Laser Assisted Micro Milling (LAMM) Processing Characteristic Titanium Alloy (Ti6Al4V) using TiAlN coated carbide micro ball mill

ICOMM 2014 No. 31

Z. Mohid[1], N. M.Warap[1], E. A. Rahim[1], M. R. Ibrahim[1], M.I.S Ismail[2]

[1] *Advanced Machining Research Group, Faculty of Mechanical and Manufacturing Engineering, Universiti Tun Hussein Onn Malaysia, 86400 Parit Raja, Batu Pahat, Johor, Malaysia*
[2] *Dep. of Mechanical and Manufacturing Engineering, Faculty of Engineering, University Putra Malaysia, 43400 Serdang, Selangor, Malaysia*

Abstract

Machining of hard-to-machine materials requires excellent cutting tool performance in terms of tool wear and life. By integrating other process such as laser as a pre-heating element in machining process, cutting force can be effectively reduced. However, applying heat from external source promotes of other defects. In addition, the microstructure of sub-surface layer prone to alter. As a result, an appropriate combination of heating temperature and machining parameters need to be determined. In this study, the heating temperature characteristics were determined numerically and validated by observing the heat affected zone (HAZ) and melted zone (MZ) obtained from experiment. The tool location and machining parameters were also determined by referring to the three dimensional temperature distribution obtained from numerical analysis. The laser heating was successfully decreased the thrust forces under certain depth of cut. The formation of melted zone and heat affected zone created by pulse wave laser significantly influence the LAMM processing characteristics.

Keywords: Laser Assisted Micro Milling (LAMM), Finite Element Analysis, Nd:YAG Laser, Titanium Alloy.

1. Introduction

Titanium and its alloys can be categorized as a hard–to-machine material. The ductile behavior of titanium alloy has become a major problem [1]. The heat generated during machining process could initiate microstructure changes thus lead to mechanical properties modification. Therefore, the machining temperature needs to be precisely controlled. In common cases, cutting fluids are used to provide cooling and chilling effect.

The heat generation during the machining process is more crucial especially when using smaller cutting tool size. The heat was conducted and transferred into the cutting tool subsequently impair its performance. However, it is proven that the generation of heat during machining process is not always unfavorable. Maintaining the machining temperature under material phase transition point is proven effective in reducing cutting force. Pre-heating the material during the machining process is effective to improve processing performance even in the case of ceramic material processing [2].

Machining process with the assistance of external heat source has been widely studied by using various heat induction methods [3] [4]. Laser is one of the heat sources used and practically applicable for localized heating area. In laser assisted micro milling (LAMM), laser irradiation is used to increase material temperature. Continuous wave laser has been successfully used to heat the workpiece surface to a constant temperature value.

It is proven that pre-heating the workpiece surface in the range of 200 to 450°C is significantly reduce the cutting force [5, 6] and prolong the cutting tool life. However, excessive temperature could give adverse effects. Furthermore, cutting tool and laser spot diameter were proven to be important in the quality of surface integrity. Using larger laser spot diameter increases the burr height and surface roughness due to material thermal softening [7].

In conventional micro milling, the minimum amount of cutting depth becomes very important. In the case of tool steel, best surface roughness can be obtained when the undeformed chip thickness is equal to the cutting tool edge radius [8]. The ratio of undeformed chip thickness to the cutting edge radius is one of the most important factor need to be considered in micro machining. In micro-scale, the plastic deformation obviously affects the workpiece surface quality. However, it can be improved if the combinations of heating and machining parameters are optimized.

Using a pulsed wave laser for heating process is generally not recommended. The peak power of each pulse generates heat instantly and chilled before the next pulsed is released. This temperature fluctuation can achieve to more than 1000 degrees of differences between maximum temperatures and chilled down temperature [9]. This will cause a sub-layer hardness modification for the solidification of melted metal. Normally, melted zones are not favorable due to the alteration of mechanical properties. However, in some cases it could be an advantage. Heat affected zone of titanium alloy poses higher hardness value which is good as corrosion protector against mechanical contact forces.

In this study, laser assisted micro milling processing characteristics of titanium alloy Ti6Al4V were evaluated. The evaluation of machining performance has been done by comparing the cutting forces obtained from LAMM and non-LAMM process

2. Analysis and experiment

2.1. Finite Element Analysis

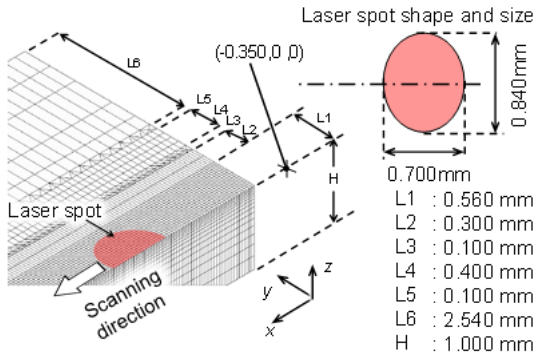

Fig. 1: Finite element model for laser scanning

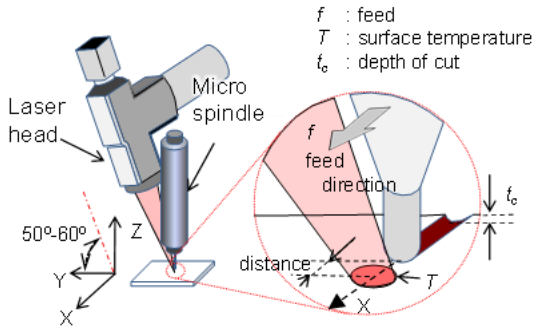

a.

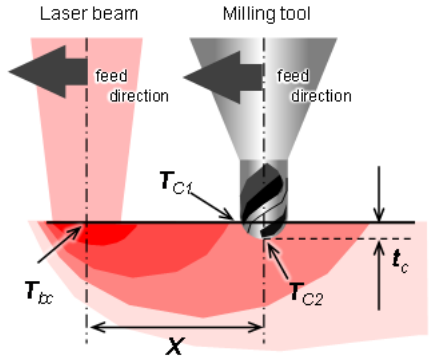

b.

Fig. 2: Cutting tool and laser beam orientation

Symmetrically half shape model with thickness, width and length of 1mm, 4.0mm and 10.8mm respectively, was developed to simulate the temperature distribution on the titanium alloy during the laser irradiation. In the model, laser beam is started 350μm behind the model and moved linearly in x-axis direction (Fig. 1).

Finite element analysis was developed and validated to predict the distribution of workpiece temperature during the irradiation process. From the simulation result, the tool engagement temperature (T_{C2} and T_{C2}), the distance between tool and laser spot ($X_{t\text{-}b}$) can be identified as shown in Fig. 2.

Table 1: Titanium alloy (Ti6Al4V) thermo-physic properties **[10]**

Temperature, *T* (K)	Thermal conductivity, *k* (W/m.K)	Heat capacity, *c* (J/(kg.K)	Density, *ρ* x 10^3 (kg/m^3)
298	7.00	546.0	4.420
373	7.45	562.0	4.406
473	8.75	584.0	4.395
573	10.15	606.0	4.381
673	11.35	629.0	4.366
773	12.60	651.0	4.350
873	14.20	673.0	4.336
973	15.50	694.0	4.324
1073	17.80	714.0	4.309
1173	20.20	734.0	4.294
1268	19.30	641.0	4.282
1373	21.00	660.0	4.267
1473	22.90	678.0	4.252
1573	23.70	696.0	4.240
1673	24.60	714.0	4.225
1773	25.80	732.0	4.205
1873	27.00	750.0	4.198
1973	28.40	759.0	4.189

Table 1 shows the material properties used in the numerical analysis. The absorption rate (*A*) of 40% to 60% for titanium alloy was employed in the simulation [11].

Simulation was started by confirming the value of laser beam Gaussian mode distribution constant (*K*). The general equation for heat flux distribution in *X* and *Y* direction is shown in Equation 1.

$$\boldsymbol{HF(x,y)} = \frac{\boldsymbol{AKP}}{\boldsymbol{S}}\boldsymbol{exp}\left[-K\frac{x^2+y^2}{b^2}\right] \quad (1)$$

A: Absorption rate (%)
K: Gaussian distribution constant
P: Laser power (W)
S: surface area (mm^2)
b: beam radius (mm)

$$HF_{all}(x,y) = HF_{surface}(x,y) + HF_{keyhole}(x,y) \quad (2)$$

Whereby the ,

$$\boldsymbol{HF_{surface}(x,y)} = \boldsymbol{K\frac{PA}{S}Q_s exp}\left\{-\boldsymbol{K}\frac{x^2+y^2}{b^2}\right\} \quad (3)$$

$$HF_{keyhole}(x,y) = K\frac{PA}{\pi r^2 \cdot H}Q_{kh}exp\left\{-K\frac{x^2+y^2}{b^2(1-\frac{z}{H})}\right\} \quad (4)$$

$$Q_{kh} + Q_s = 1 \quad (5)$$

Q_{kh} and Q_s: Key hole and surface heat flux ratio
r : keyhole radius
H : key hole depth
Z : distance in z axis from top surface

In the case of keyhole generation, the heat is induced into the workpiece in three dimensional directions. Equation 2 will be applied if the heat energy is induced into the workpiece top surface and keyhole side surface.

From the experiment, the existence of keyhole can only be confirmed by observing in the cross

sectional direction of the melted zone (MZ). By ignoring the existence of keyhole, total heat flux can be written as,

$$HF_{all}(x,y) = K\frac{PA}{S}exp\left\{-K\frac{x^2+y^2}{b^2}\right\} \quad (6)$$

2.2. Micro milling process.

The experiment was conducted on a table-top micro milling machine. This machine was equipped with an air bearing spindle and attached on the Z axis together with a laser processing head. The laser processing head is fixed at 55° inclination angle from X-Y plane.

Micro ball milling tool with nominal diameter of 0.3mm was used to produce a linear line grooving. The tool was selected for the capability of hard material cutting process [12]. The tool overhang was kept constant at 17mm. Linear grooving process with the distance of 25mm was performed repeatedly and the tool was inspected after each path. The grooving lines were then inspected to confirm their location against the laser scanning path and to compare the cutting condition among different machining parameters.

The distance between the cutting tool to the centre of laser spot was defined based on the temperature distribution obtained from numerical analysis. The maximum depth was determined from laser irradiation experiment by considering the maximum depth of HAZ. From the numerical analysis, the workpiece material temperatures were in the range of 370K to 500K at the distance of 1mm from the centre of laser beam spot. Thus, in the LAMM experiment, cutting tool was set according to this distance.

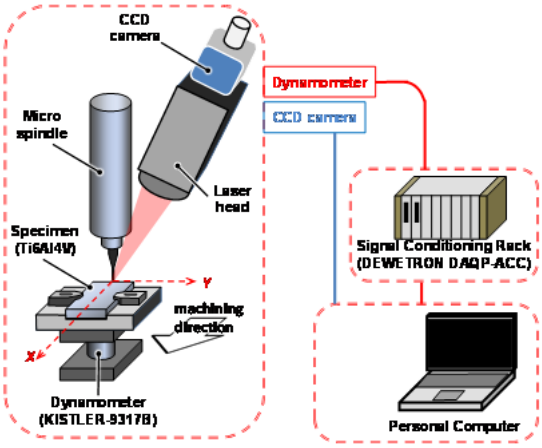

Fig. 3: Schematic diagram of experimental setup

The effectiveness of LAMM was evaluated by comparing its result to conventional micro milling (non-LAMM). Fig. **3** shows the schematic diagram of experimental setup. A titanium alloy plate is fixed on a holding jig which is mounted on a tool dynamometer. The depth of cut was controlled by tool setter with measuring pressure 0.2 Newton (NISSIN i-50). Tool dynamometer with measurement area of 25 x 25mm^2 was used to measure the cutting force. The cutting forces were recorded using personal computer through charge amplifier embedded in a signal conditioner rack. Table 3 shows the machining parameters used in LAMM and conventional micro milling process.

Table 2: Cutting tool specification

Items	Specification
Tool material	Cemented carbide
Tool type	Ball end mill
Tool diameter, $Ø_{t\_max}$ (mm)	0.3
Flute number	2
Coating material	TiAlN

Table 3: LAMM and without laser assist micro milling (non-LAMM) processing experiment parameter

Parameters	Experiment setting value
Laser average power, P_{avg} (W)	14
Pulse repetition rate, f_p (Hz)	100
Pulse width, t_p (ms)	1
Table speed, v_f (mm/min)	210
Spindle rotation speed, N (RPM)	40,000
Depth of cut, t_c (mm)	0.030 to 0.110

3. Results and Discussion

3.1 Thermal analysis

From the numerical analysis (Fig. 4), the width and depth of HAZ and MZ were obtained by referring to the temperature distribution boundary line. The HAZ areas were determined at the 1253*K* temperature line, while the MZ areas were determine at the 1933*K* temperature line [10]. The HAZ and MZ from the laser scanning experiment were measured from cross sectional direction at location 20mm from irradiation start point.

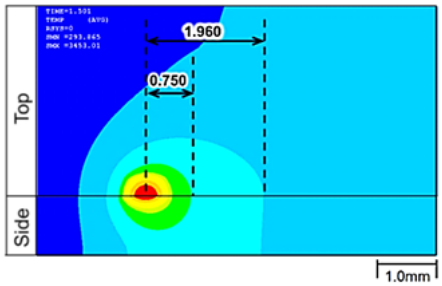

a. Analysis (top and side view

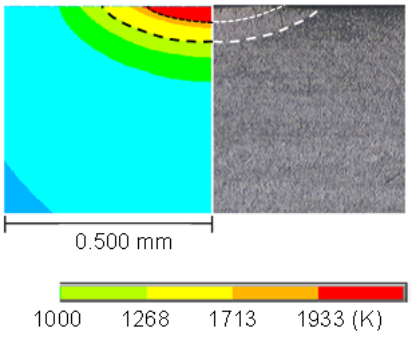

b. Cross section view (analysis and experiment)

Fig. 4: Result for laser scanning **[9]** (f_p=100Hz, t_p=1ms, P_{avg}=14W, v_f=210mm/min)

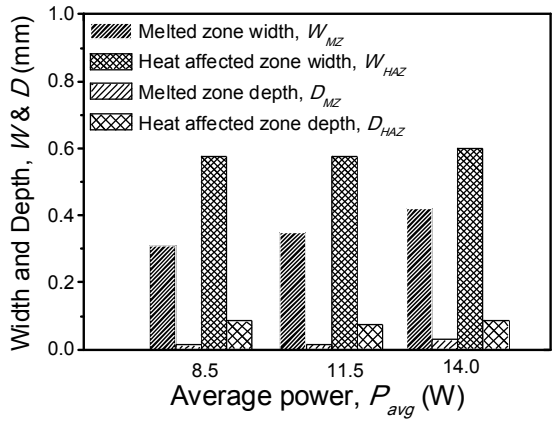

Fig. 5: HAZ and MZ measurement obtained from experiment

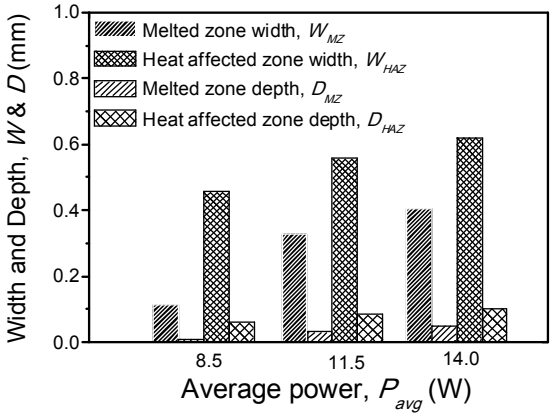

Fig. 6: HAZ and MZ measurement obtained from finite element analysis

Fig. **5** and Fig. 6 show the measurement of HAZ and MZ under different laser average power (P_{avg}). The result obtained from numerical analysis are well agrees with the experiment result when the P_{avg} of 14.0W and 11.5W were applied. In the case of P_{avg} of 8.5W, overall measurement of HAZ and MZ were smaller than the actual experiment. The variation the the result was due to the assumption considered in the numerical analysis.

The pulse was assumed to be on and off immediately in straight vertical lines, meanwhile the pulse duration (t_p) was considered as the same as to be actually same to the nominal setting value. The actual peak power value could be higher from the scanning setting value. The stability of irradiated laser beam power per each pulse also contributes to the HAZ and MZ measurement.

3.2 Laser Assisted Micro Milling

The machined surfaces were then analysed using microscope with 200 times magnification. From cross sectional direction, the microstructure changes and the developed burrs at the groove circumference area was observed to study the influence of laser irradiation in LAMM process.

Single line grooving was performed under constant laser average power and table feed (P_{avg} = 14W, v_f= 210mm/min).

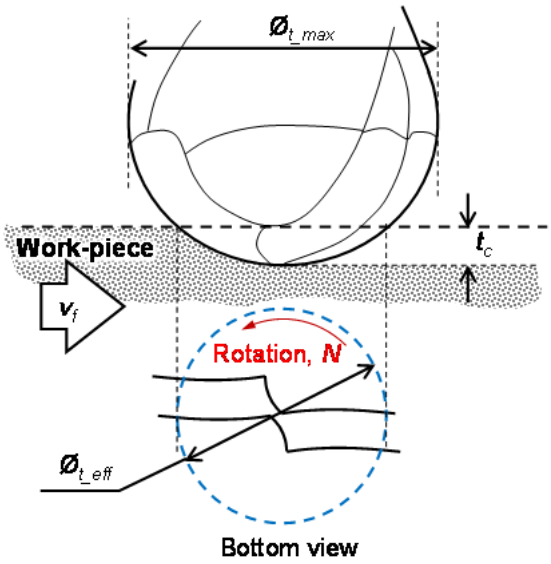

$Ø_{t\_eff.}$: tool effective diameter (mm)
$Ø_{t\_max.}$: tool maximum diameter (mm)
t_c : grooving depth (mm)
N : tool rotation speed (rpm)
v_f : table speed (mm/min)

Fig. 7: Schematic diagram of cutting tool engagement

Experimentally, it has been clarified that the depth (D_{MZ}) and width (W_{MZ}) of melted zone are approximately 30 and 370µm respectively, whilst the depth (D_{HAZ}) and the width (W_{HAZ}) of heat affected zone are approximately 90µm and 570µm respectively. Four different grooving depths results at four different tool effective diameters. It was observed that at shallow grooving depth, the remaining HAZ and MZ were larger compared to the deeper grooving depth (Fig. 7).

Actual groove size and shape were observed from cross sectional direction for booth LAMM and non-LAMM. The laser scanning line and the tool moving paths were also confirmed that they were performed at the same position (Fig. 8).

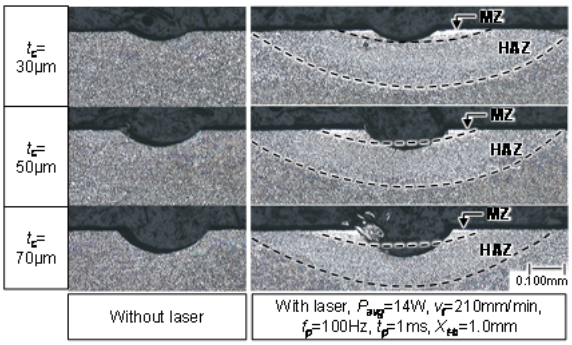

Fig. 8: Laser scanning and groove cutting position confirmation with different depth of cut

For each processing conditions, the tools were observed using visual microscope. After 25mm cutting distance, it was observed that the cutting tool edge suffered from adhesion wear mechanism especially at the rake surface as shown in Fig. 9-a.

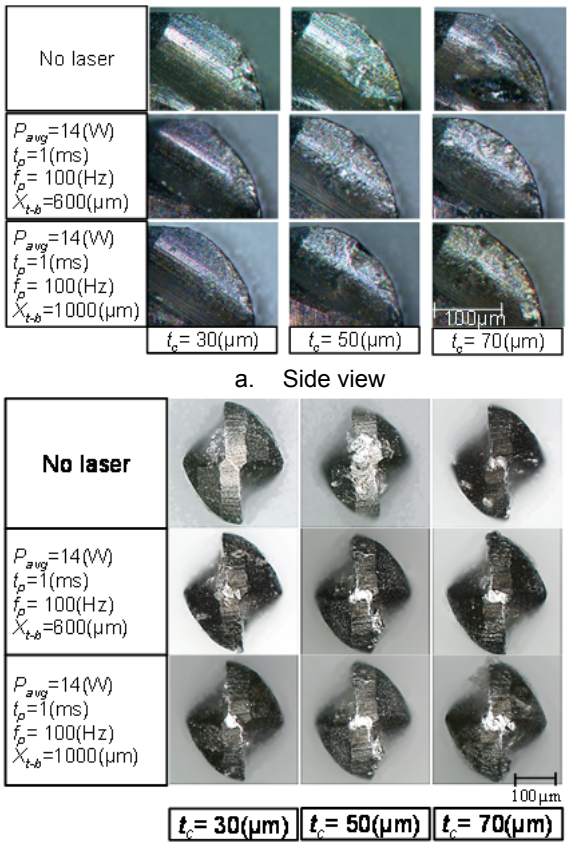

a. Side view

b. Top view

Fig. 9: Cutting tool condition after 25mm groove cutting process

This phenomena contributes to the inconsistence of machining performance. In addition, the fluctuation value of thrust force was due to the adhered material at the bottom-centre of cutting tool (Fig. 9-b). Temporarily, adhered material on the cutting edge promoting the blunt cutting edge. The cutting edge radius effect and plunging effect dominate the cutting mechanism [13]. This phenomenon happens during non-LAMM and LAMM process. At cutting distance of 75mm, there were no obvious chipping or tool wear can be identified.

Fig. 10 compares the cutting forces between different depth of cut under the non-LAMM process. It can be observed that the cutting force increases as the cutting depth (t_c) increase. However, when the laser irradiation is applied in the process, the recorded cutting forces were contradicted with non-.

As shown in Fig. 10, the F_x and F_y were slightly increased in the case of laser assisted micro milling with tool to laser beam distance X_{t-b} was 1.0mm. However, in the case of X_{t-b} was 0.6mm, the thrust force decreases to 2N at the depth of cut of 50μm. Furthermore, it gradually increases to nearly 3N when the t_c increased to 110μm. It can be suggested that the constant value of D_{MZ} and D_{HAZ} (Fig. 11) contributed to the variations of cutting force.

Irradiating the specimen using P_{avg} and v_f of 14W and 210mm/min respectively, has created melted zone with the depth approximately 30μm.This *MZ* layer is harder compared to the other region. Performing LAMM at t_c equal or less than D_{MZ} has consequently allows the cutting tool to travel on a harder material surface.

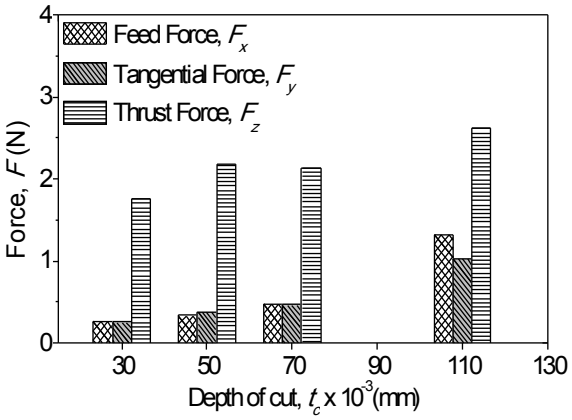

Fig. 10: Cutting forces for non-LAMM

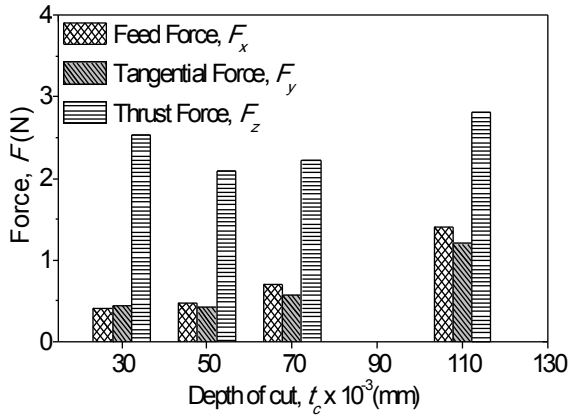

Fig. 11: Cutting forces when X_{t-b}= 1.0(mm)

The creation of MZ is hard to be avoided especially when pulsed mode laser is applied. This mode emits the laser beam with high peak power. It is suggested that higher pulse repetition rate is better to reduce the thickness of melted zone and heat affected zone.

When the t_c is increased to 50μm, the centre part of the tool which does not have cutting edge was not running on the hardened surface (Fig. 12). This has consequently reduced the thrust force. However, when the depth is increased to more than 70μm, the thrust force was gradually increased. This is due to the increment of tool-material contact surface for the tool effective diameter increment.

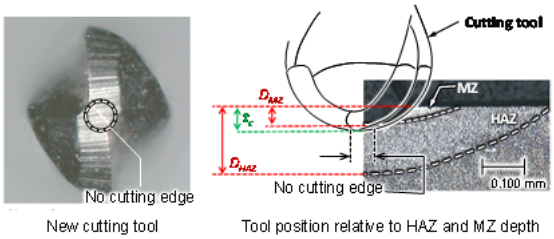

Fig. 12: Cutting tool design and cutting depth effect

From the results obtained, it can be concluded that the LAMM does not effectively reduce the cutting forces. The hardness of material increases just before the cutting tool arrives. Considering the hardness increment, the cutting tool engagement temperature needs to be increased for better softening effect on the workpiece surface. However, the maximum heating temperature needs to be controlled under phase transformation temperature to

avoid undesirable material hardening effect.

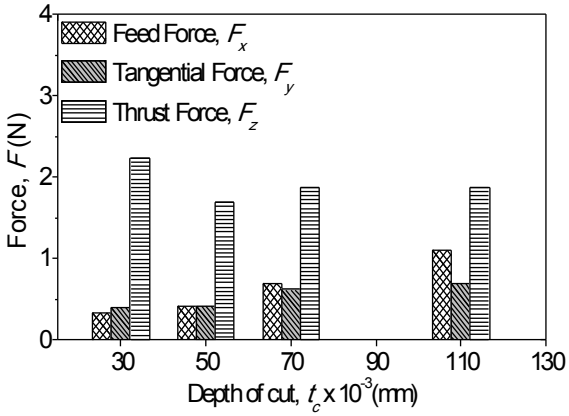

Fig. 13: Cutting forces when $X_{t\text{-}b}$= 0.6(mm)

Fig. 13 shows the result of cutting forces when the cutting tool is located closer to the laser beam spot position. It is found out that the thrust force decreased when the $X_{t\text{-}b}$ is reduced. Thrust forces measured at all t_c value were recorded in lower values. However, the other two force elements were increased with the t_c. Comparing Fig. 11 and Fig. 13, it can be concluded that cutting force can be reduced by minimizing the tool-to-beam distance.

4. Conclusions

From the numerical analysis and experimental works, it can be concluded that:

i. Pulse wave Nd:YAG laser creates high temperature fluctuation. The existence of melted zone could not be clearly eliminated for the Gaussian beam intensity distribution.
ii. The location of cutting tool and the range of cutting depth can be determined using numerical analysis validate by experiment melted zone and heat affected zone size.
iii. In the case of non-LAMM, thrust force increases with the depth of cut. However, in the case of LAMM, the cutting force decreases when the depth of cut is larger than the melted zone depth. Then, it increased gradually with the increment of depth of cut.
iv. The adhered workpiece material in the machined groove surface increases when the depth of cut is increase.
v. The creation of melted zone when heating using pulse wave laser has significant effect to the LAMM performance. Re-solidified layers created just before the cutting tool engagement has caused chipping on the cutting tool cutting edge.

Acknowledgements

This study is sponsored by Ministry of Science, Technology and Innovation of Malaysia under Science Fund Research Grant (S020). Micro-ball mill cutting tools were supplied by Mitsubishi Materials, Japan.

References

[1] E. A. Rahim and H. Sasahara, "A tudy of the effect of palm oil as MQL lubricant on hig speed drilling of titanium alloys," *Tribology International,* vol. 44, pp. 309-317, 2011.

[2] C. W. Chang and C. P. Kuo, "Evaluation of surface roughness in laser-assisted machining of aluminum oxide ceramics with Taguchi method," *International Journal of Machine Tools & Manufacture,* vol. 47, pp. 141-147, 2007.

[3] K. Maity and P. Swain, "An experimental investigation of hot-machining to predict tool life," *Journal of Materials Processing Technology,* vol. 198, pp. 344-349, 2008.

[4] L. Ozler, A. Inan and C. Ozel, "Theoretical and experimental determination of tooll in hot machining of austenitic manganese steel," *Journal of Machine Tools & Manufacture,* vol. 41, pp. 163-172, 2001.

[5] S. Sun, M. Brandt, J. E. Barners and M. S. Dragusch, "Experimental investigation of cutting forces and tool wear during laser-assisted milling of Ti-6Al-4V alloy," in *Proceedings of the Institution of Mechanical Engineers, Part B: Journal of Engineering Manufacture 225: 1512-1527*, 2011.

[6] R. D. Chinmaya, Y. C. Shin and J. Barnes, "Machinability improvement of titanium alloy (Ti–6Al–4V) via LAM and hybrid machining," *International Journal of Machine Tools & Manufacture,* vol. 50, pp. 174-182, 2010.

[7] M. Kumar and S. N. Melkote, "Process capability study of laser assisted micro milling of a hard-to-machine material," *Journal of Manufacturing Processes,* vol. 14, p. 41–51, 2012.

[8] A. Aramcharoen and P. T. Mativenga, "Size effect and tool geometry in micromilling of tool steel," *Precision Engineering,* vol. 33, pp. 402-407, 2009.

[9] Z. Mohid, N. H. S. Warap, M. Ismail, R. Ibrahim and E. Rahim, "Numerical Analysis of Laser Heating for Laser Assisted Micro Milling Application," *Applied Mechanics and Materials,* Vols. 465-466, pp. 720-724, 2014.

[10] J. Yang, S. Sun, M. Brandt and W. Yan, "Experimental investigation and 3D finite element prediction of the heat affected zone during laser assisted machining of Ti6Al4V alloy," *Journal of Materials Processing Technology,* vol. 210, pp. 2215-2222, 2010.

[11] M. F. Zaeh, R. Wiedenmann and R. Daub, "A Thermal Simulation Model for Laser-Assisted Milling," *Physics Procedia,* vol. 5, p. 353–362, 2010.

[12] A. Aramcharoen, P. T. Mativenga, S. Yang, K. E. Cooke and D. G. Teer, "Evaluation and selection of hard coatings for micro milling of hardened tool steel," *International Journal of Machine Tools & Manufacture,* vol. 48, pp. 1578-1584, 2008.

[13] G. Bissacco, H. Hansen and J. Slunsky, "Modelling the cutting edge radius size effect for force prediction in micro milling," *CIRP Annals - Manufacturing Technology,* vol. 57, pp. 113-116, 2008.